HYPERBOLIC RETRACKER: REMOVING BRIGHT TARGET ARTEFACTS FROM ALTIMETRIC WAVEFORM DATA

Graham D. Quartly

National Oceanography Centre (NOC), Empress Dock, Southampton, Hants, UK: gdq@noc.soton.ac.uk

ABSTRACT

Over a homogenous surface such as the ocean, the expected radar return (waveform) has a simple smooth shape from which estimates of range and wave height are readily derived. This is accomplished by fitting a simple parametric description to the waveforms. Occasionally strong reflections exist above the sea surface, generating a spurious echo that follows a hyperbolic trajectory through waveform space. This paper shows the simulation of such features, the estimation of signal strength and the removal of features as a precursor to the application of conventional waveform retrackers. For these small coherent reflectors, the phase information available in the RA-2 individual echoes shows much greater coherence than for extended ocean targets.

1. INTRODUCTION

The radar echo recorded by a radar altimeter is the sum of the returns from the many reflecting facets within the footprint. For a homogeneous isotropic surface the expected shape can be expressed as the convolution of three terms: the Point Target Response (effectively the emitted signal), the Flat Surface Response (delayed contributions from points lying further from nadir) and the variability in surface elevation (which is usually expressed in terms of significant wave height, H_s). The actual signal at a particular time delay and recorded in an individual waveform bin, is the sum of multiple facets lying in an annulus around the nadir point (Fig. 1a). As the phase shift of such reflecting facets varies randomly over $[0,2\pi]$ the complex addition of these returns may interact constructively or destructively, such that the actual signal amplitude at a particular bin will vary considerably from the form shown in Fig. 1b. The addition of 100 such pulses (0.05s for the RA-2 on Envisat) markedly reduces the observed variability in each bin (Fig. 1c).

Reflecting points above the sea surface may give earlier returns. Although such points are generally not as strong reflectors as large areas of the sea, their contributions to the echoes may be noticeable, simply because they exceed the background level due to thermal noise in the instrument's detector. Tournadre [1] showed various examples due to lighthouses and ships, and subsequently developed a routine for automatically detecting such early returns, and used it to study the heights of icebergs in the Southern Ocean [2]. This paper uses a different approach, showing the simulation of such early returns, and how such anomalies may be removed from the waveform record.

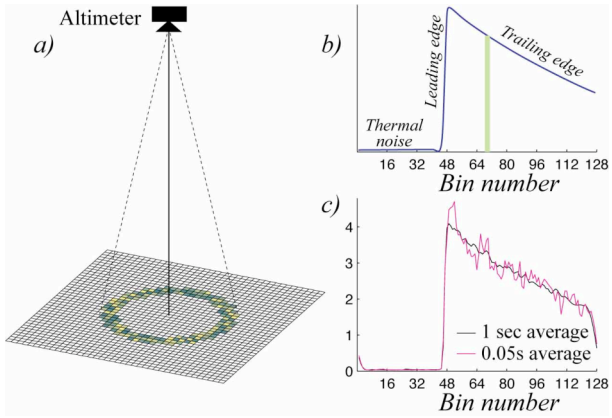

Figure 1. Radar return from a homogenous isotropic surface. a) Schematic showing annulus of points at similar path delay. b) Idealised waveform, with tail off in power due to antenna beamwidth. Wave height is determined from the slope of the leading edge. c) Real RA-2 waveforms, including fading noise.

2. SIMULATIONS

The simulation work is based on ideas used in the simulation of radar returns attenuated by intervening rain cells [3,4]. In essence the altimeter traverses a grid of small pixels, and those within the prescribed range contribute to the summation, with their contribution weighted by a function of wave height (as the range in elevation of reflecting facets within a pixel will span many bins).

2.1. Equations for path delay

The earliest returns from the mean sea surface occur for reflections from nadir. For a point at distance ρ from nadir, and at height, h, above the sea surface, Quartly [3] showed that the extra path length relative to the nadir reflection, ξ (see Fig. 2), is given by

$$(H + \xi)^2 = (H - h)^2 + \rho^2 \qquad (1)$$

where H is the reduced height of the satellite (given by $H^{-1} = H_0^{-1} + r_E^{-1}$, H_0 being the true height and r_E the

radius of the Earth). Eq. 1 describes a hyperbola, but as H>>ρ>>h this reduces to a parabola:

$$\xi = \rho^2 / 2H - h \qquad (2)$$

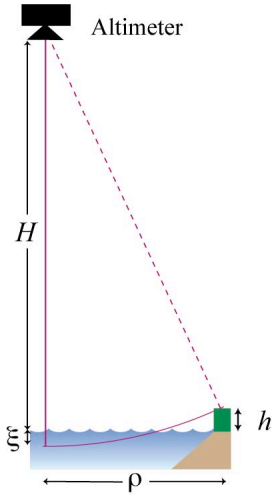

Figure 2. Schematic showing extra path delay, ξ, to a point h above sea level, but at distance ρ from nadir.

If the altimeter, travelling at speed v, passes close to the high reflector at time t_0, then the distance, ρ, varies with time as:

$$\rho^2 = x_0^2 + v^2 (t-t_0)^2 \qquad (3)$$

where x_0 is the distance at nearest approach. The path delay, ξ, is converted to waveform bin relative to nadir reflection, k, by dividing by $c\Delta t/2$, where c is speed of propagation of radio waves, Δt is the time interval corresponding to each waveform bin, and the factor of 2 allows for two-way travel time. Consequently, the echo of a simple small target will follow a simple curve in waveform space given by

$$k = \frac{x_0^2 - 2hH}{H\, c\Delta t} + \frac{v^2 (t-t_0)^2}{H\, c\Delta t} \qquad (4)$$

Thus small bright targets always produce the same shape curve, with the only parameters to be determined relating to the location of the apex along track, and by how much this localised return precedes/lags behind the return from the sea surface at nadir. In practice, such small raised targets will not be discernible unless they have some effect in front of the leading edge. The key things to notice are that the bin number of the apex is a summation of the effects of height above surface and distance from nadir, and that these two factors cannot be separated using the data from a single transit.

2.2. Implementation

For the RA-2 altimeter on the Envisat platform, H_0=780 km, Δt=3.125ns, v=6.7 km s^{-1}, average waveforms come at intervals, δt of 0.057s, and the waveform reception window is adjusted to position the nadir return (half-power point on leading edge) at bin 46. To simulate sea surface returns as far as bin no. 128, the grid must extend to at least 7 km from the sub-satellite point. To achieve the expected smooth curve for the trailing edge, a pixel resolution of no more than 40m was adopted. The contributions from different pixels are added incoherently i.e. reflected power is summed, rather than including phase information. After some tuning of parameters (to include width of emitted pulse as well as smearing effects due to wave height), the simulated curve for a uniform surface closely matches the average of many seconds of RA-2 data.

In the marine environment, most cases of above-sea targets are small — ships, rocky outcrops on small islands etc. — with a size smaller than the distance $v\delta t$ travelled between successive average waveforms. [The more complicated situation of the altimeter approaching a large land mass is not treated here, as then there are an amorphous collection of disparate reflections, and consequently much movement of the waveform reception window.] In the simulations conducted here, individual bright targets are less than 100m in size.

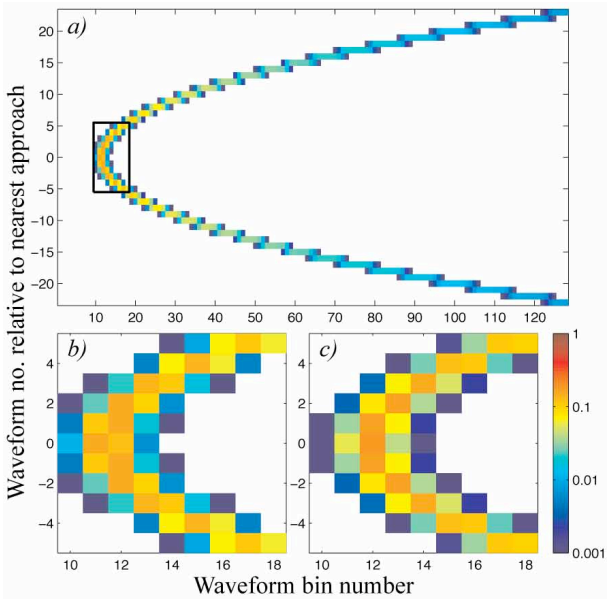

Figure 3. Simulation of small bright targets (with sea surface omitted). a) 2-D representation for case 1. b) Close-up near apex. c) Close-up near apex for case 2 (lower in height than case 1 by 23 cm). All plots are displayed in same arbitrary units with a logarithmic colour scale.

2.3. Resulting hyperbolae

The 2-D pattern of the simulated radar echoes for a discrete bright target (Fig. 3a) has the expected hyperbolic shape, with the power decreasing notably away from the apex, due to the signal then being spread over multiple waveform bins. The position of the apex relates to the position of the reflector above mean sea level (Eq. 4), such that a decrease in height by $c\Delta t/2$

translates the display one bin to the right. Figs. 3b,c show close-ups of the apex for simulations differing in height by $c\Delta t/4$ i.e. 23.4 cm.

3. DETECTING AND LOCALISING HYPERBOLAE

In the absence of any other signals it is relatively straightforward to develop a filter to locate these characteristic curves within waveform data. By not considering transits over large land masses, it is realistic to assume that the number of discrete reflectors present is few. Thus a simple approach is to use a 2-D filter comprising of a normalised version of the signal strength near the apex, and then iteratively select the best match and remove that contribution. Because the hyperbolae for discrete reflectors at similar delays overlap (Figs. 3b,c), a filter designed for the first case will locate the peak in the second case. However then the subtracted signal will not completely match the original.

Fig. 4b illustrates the result of fitting the case 1 model to a simulation using case 2. The hyperbola amplitude is underestimated by ~10%, and the removal of this slightly staggered facsimile leaves a pair of curves of contrasting sign, but much reduced amplitude compared with the original (Fig. 4a). This demonstrates that to achieve a clean removal of the strong reflector, it is essential to use a set of normalised filters, each allowing for minor offsets in location, and then determine the optimum match.

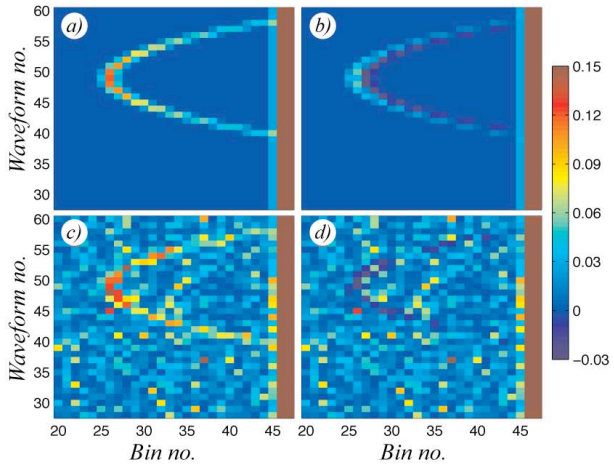

Figure 4. Recovery of echo from a raised target (case 2) plus an ocean signal (of unit amplitude). a) Pure signal. b) Result of fitting and removing case 1 model. c) Addition of exponential noise (mean=0.02). d) Result of fitting case 2 model to noisy signal.

Fig. 4c shows a simulation with thermal noise added, with Fig. 4d showing the residual after fitting using the correct model. The noise leads to a slight overestimate of the hyperbola strength and thus minor negative residuals.

4. PIANOSA CASE STUDY

The small island of Pianosa in the Tuscan archipelago has received considerable altimetric attention recently, because the Envisat pass that crosses the island has shown the intermittent occurrence of an extended bright target in its northern bay [5]. Such a bright target corresponds to a path delay similar to that at nadir, and over an extended area; therefore Gómez-Enri et al. [5] concluded it to be due to a modulation of the sea surface roughness, possibly associated with the sheltering from the winds afforded by the northern peninsula.

Closer examination of one of the particular overflights shows two hyperbolae (Fig. 5a), with the apex of the more distant one lying a little further south (earlier waveform no.). A simple model of surface backscatter strengths using a precise DEM (digital elevation model) for the island (assumed weak backscatter strength) plus a disc of enhanced backscatter (calm seas) occupying the northern and eastern bays (Fig. 5b) produces a good facsimile (Fig. 5c) of the received RA-2 waveforms.

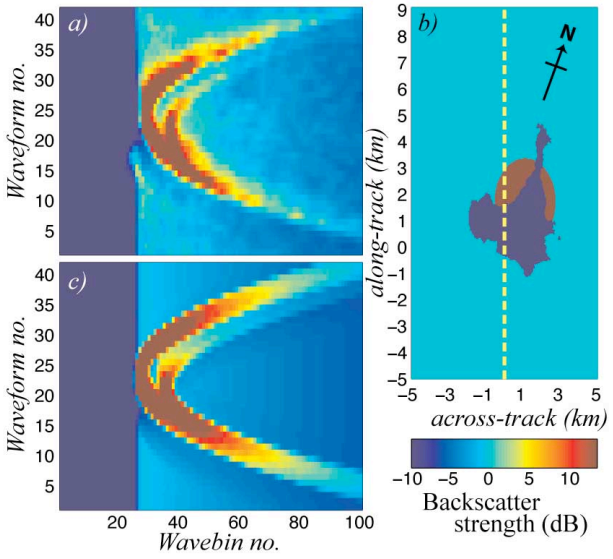

Figure 5. a) RA-2 K_u-band waveforms for track 128 across Pianosa (42˚35'N, 10˚04'E) on 5th July 2006. b) backscatter strength for simulation (on a grid aligned with altimeter track (yellow dashed line). c) Result of simulation.

Pianosa has an area of ~10km^2, and is generally vegetated so K_u-band reflections from the island itself are weak. However, by focussing on the early bins ahead of the leading edge, hyperbolae can be seen (Fig. 6). Seven such repeat passes are displayed, with all showing a series of concentric arcs, presumably due to different points at the same latitude providing discrete

targets. Envelope curves (shown in pink) are fitted using a thresholding technique, with the axes of the first plot expanded to show the location of the apex. These envelopes have been automatically fitted to 28 passes of waveform data (20th Feb 2005 to 30th Nov 2007). The strength of the signal (after AGC setting applied) varies by more than a factor of 10. In all cases the automated technique fitted an envelope, though for the weakest ones the robustness of the fit is uncertain.

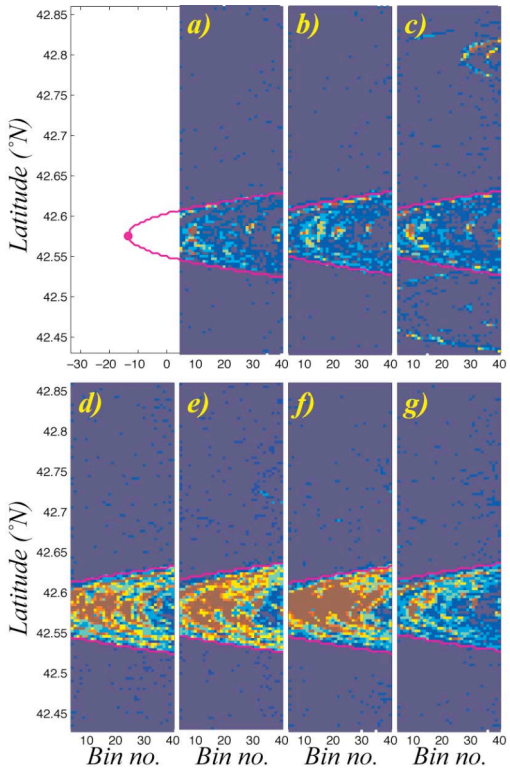

Figure 6. Pre-leading edge waveform data for 7 repeats of track 128 near Pianosa, with fitted curve to show envelope of surface reflections. a)-g) are cycles 071 to 077 respectively.

The co-ordinates of the apex of the fitted envelope define the latitude and height of reflector (assumed on satellite track). The results for the last 20 (cycles 56 to 77, spanning Mar. 2007 to Mar. 2009) are shown in Fig. 7. Initial estimates are that the nearest land point to the altimeter i.e. the point on the island's ridge underlying the satellite track) is at a latitude of 42.5792° (s.d.=0.0027°), with a height of 28.2m (s.d.=1.6m). The high-resolution DEM has the satellite crossing the ridge at 42.5817°N, where the height is 26.5m. Although the height values derived from the altimeter waveform are close to this, it is possible that some algorithm bias still exists. Future work will examine the processing more fully. However, the conclusion is that, by using many repeat passes, the peaks of small islands can be retrieved to an accuracy of ~1-2m, even when the principal return signal is from the ocean.

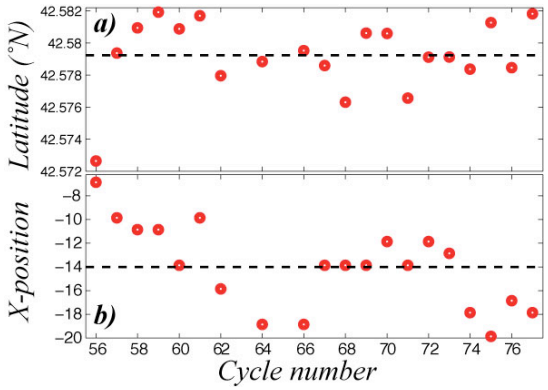

Figure 7. Locations of the fitted envelope for repeat cycles 56 to 77. a) Waveform no. converted to latitude. b) Wavebin number (see Fig. 6a for interpretation of negative nos.)

5. SUMMARY AND IMPLICATIONS

A realistic waveform simulator has been developed and used to replicate the finely detailed curves occasionally seen in ocean returns ahead of the leading edge. These signals are usually much weaker than the ocean signal (which emanates from a much larger area), but when close to the leading edge may complicate the application of a standard "Brown" ocean retracker. Such concern about bright targets has led to the development of "mixed" retrackers that include potential specular returns in the parameterized description of the waveform [6]. The technique developed here will enable the estimation and removal of discrete bright targets occurring before the leading edge, and thus reduce the need for such a complicated retracker.

An important by-product of this work is an automatic quantitative estimation of the height of salient features. Tournadre has developed a similar approach, with convolution with a pre-determined set of weights, and used that to create a census of iceberg heights [2]. The evaluation of this new approach over islands allows a more detailed investigation of the errors in such retrievals, and, critically, the technique now copes with islands higher than 18m and thus whose envelope of reflection points has an apex before the start of the waveform reception window (sect. 4). An interesting side issue is that many of the small bright targets identified by this work offer interesting opportunities to evaluate our understanding of the phase relationships in the complex individual echoes (see appendix)

6. APPENDIX: ANALYSIS OF INDIVIDUAL ECHOES

The RA-2 collects 1-sec "bursts" of individual echoes (IEs) every 3 minutes along orbit. These bursts contain 1984 waveforms as complex data (both amplitude and phase). These data firstly offer processing at a higher

spatial resolution, and secondly the opportunity to derive new information not available when signals have already been averaged incoherently. Fig. A1 shows a particular burst in the Mediterranean close to Port Said. The amplitude data have been averaged in groups of 20 (as opposed to groups of 100 for the normal 18 Hz waveforms): four partial arcs of hyperbolae can be discerned. It is highly likely that these are large ships (such as oil tankers) entering/exiting the Suez Canal.

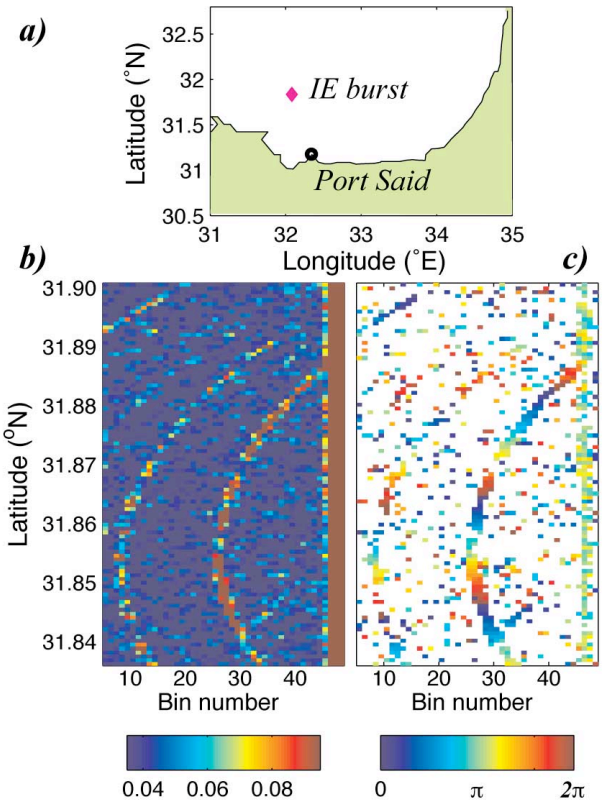

Figure A1. Analysis of a 1-sec burst of IEs in SE Mediterranean. a) Location, b) Amplitude in early (pre-leading edge) bins, averaged in groups of 20, c) Phase difference between successive waveforms (averaged in groups of 20, with significance test applied).

Phase information is much more complicated to interpret, as all values in the span [0,2π] are equally likely. However, the difference between successive pulses may be coherent. Although the sub-satellite point moves 3.7m between consecutive IEs whilst the radar wavelength is 2.2 cm, the actual path length from altimeter to a reflector close to nadir will only be slowly changing. Fig. A1c shows the result of vector averaging these phase differences in groups of 20, displaying only those that show a clear coherency. This highlights several of the arcs seen in Fig. A1b, without making any use of the amplitude information. There is also a line of consistent phase change around bin 44 at the start of the leading edge when the disc on the ocean contributing to the echo is small. The phase difference here is close to π, but oceanographic interpretation awaits further comprehension of the on-board processing of IEs.

A further set of examples occurs at the mouth of the Yangtze river near Shanghai (Fig. A2). (Burst locations are the same in each 35-day cycle as the 3-minute sampling is re-initiated in every cycle to make them coincident.) The waveform leading edge (red band on right-hand side of amplitude plots) shows much movement as the tracker is still responding to the preceding seconds' travel over land. A complicated set of concentric bright targets can be seen, presumably due to the land to the south of the river. Calculation of the phase difference again shows these reflective points to offer a strong coherency in phase. This is very different to reflections over the ocean itself, where phase changes are, in general, much more variable due to movement of the reflecting facets between pulses.

7. ACKNOWLEDGEMENTS

The 18 Hz waveform data were obtained from ESA through the Cat-1 proposal ARIES (*Accurate Rain Information from Envsiat Sensors*) and the IEs under the project RAIES (*Radar Altimeter Individual Echoes and S-band*). this work has been supported by ESA through the COASTALT programme (http://www.coastalt.eu).

8. REFERENCES

[1] Tournadre J., Signature of lighthouses, ships, and small islands in altimeter waveforms, *J. Atmos. Oceanic Tech*. 24, 1143-1149, 2007.

[2] Tournadre J., K. Whitmer, and F. Girard-Ardhuin, Iceberg detection in open water by altimeter waveform analysis, *J. Geophys. Res*. 113, art. no. C08040, 2008.

[3] Quartly G.D., Determination of oceanic rain rate and rain cell structure from altimeter waveform data. Part I: Theory, *J. Atmos. Oceanic Tech*. 15, 1361-1378, 1998.

[4] Quartly G.D., M.A. Srokosz and T.H. Guymer, Understanding the effects of rain on radar altimeter waveforms, *Adv. in Space Res*. 22, 1567-1570, 1999.

[5] Gómez-Enrí, J., S. Vignudelli, G.D. Quartly, C.P. Gommenginger, P. Cipollini, P.G. Challenor and J. Benveniste, Modeling Envisat RA-2 waveforms in the coastal zone: Case-study of calm water contamination, *IEEE Geosci. Rem. Sensing Lett.* 7 (3), 474-478, 2010.

[6] Gommenginger, C.P. et al. Retracking altimeter waveforms near the coasts A review of retracking methods and some applications to coastal waveforms, in *Coastal Altimetry* [ed. Vignudelli S. et al.] Springer, 2010.

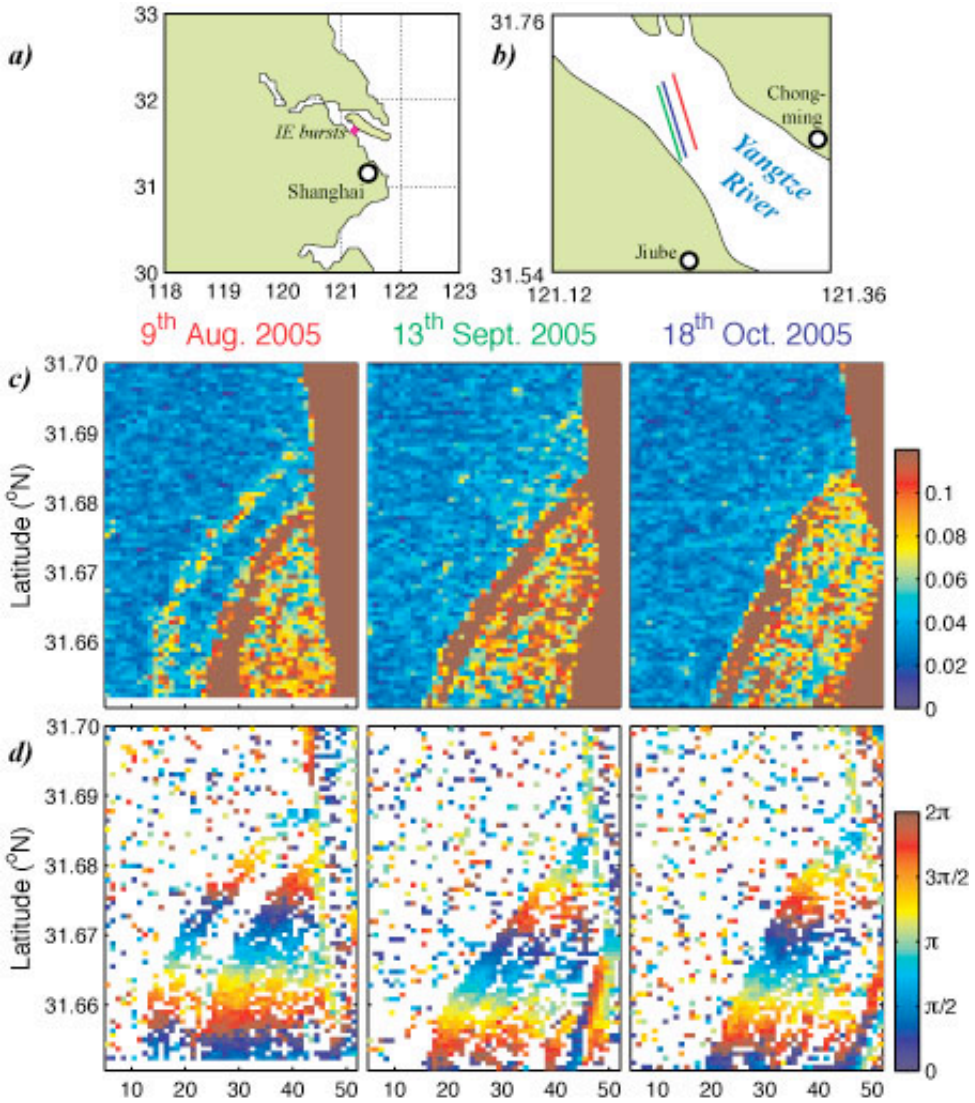

Figure A2. Analyses of three separate 1-sec bursts of IEs at the mouth of the Yangtze River. a) Location to NNW of Shanghai. b) Zoomed in plot showing locations of the three bursts. c) Amplitude in early bins, averaged in groups of 20, c) Phase difference between successive waveforms (averaged in groups of 20).